Supporting Information (SI)

FM dyes enter via a store-operated calcium channel and modify calcium signaling of cultured astrocytes

Dongdong LI, Karine HERAULT, Martin OHEIM, and Nicole ROPERT

INSERM, U603, Paris, F-75006 France; CNRS UMR 8154, Paris, F-75006 France; Université Paris Descartes, Laboratoire de Neurophysiologie et Nouvelles Microscopies, Paris, F-75006 France.

SI contains:

- List of Abbreviations
- Supplementary Experimental Procedures
- Supplementary References
- 3 Supplementary Tables
- 10 Supplementary Figures

List of abbreviations

2-APB	2-aminoethoxy diphenylborate
AChR	acetylcholine receptor
AMPA	α-amino-3-hydroxy-5-methyl-4-isoxazolepropionic acid
AA	arachidonic acid
AM	acetoxymethyl ester
Aniso	anisomycin
ATP	adenosine-5'-triphosphate
BAPTA	2,2′-(Ethylenedioxy)dianiline-*N,N,N′,N′*-tetraacetic acid
Bfa	brefeldin A
BPB	bromophenol blue
BTP2	3,5-bistrifluoromethyl pyrazole 2
Ca^{2+}	calcium
Caf	caffeine
Caly	calyculin A
CBX	carbonoxolone
CES-2	carboxylesterase-2
CNS	central nervous system
CTR	control
D-AP5	D-(-)-2-amino-5-phosphonopentanoic acid
DHS	dihydrostreptomycin
Dyn	dynamin
EGTA	ethylene glycol-bis(2-aminoethylether)-N,N,N′,N′-tetraacetic acid
EPI	epifluorescence
ER	endoplasmic reticulum
FFA	flufenamic acid

FL-d	fluorescein dextran
FWHM	full width at half maximum
Gd^{3+}	gadolinium
GsMTx-4	*Grammostola spatulata* mechanotoxin peptide 4
h-Ca	high calcium
IP_3R	inositol trisphosphate receptor
$iPLA_2$	Ca^{2+}-independent phospholipase A_2
Jasp	jasplakinolide
KB-R-7943	2-[2-[4-(4-Nitrobenzyloxy)phenyl]ethyl]isothiourea mesylate
LPC	lysophosphatidylcholine
MβCD	methyl-β-cyclodextrin
MF	single-cell mean fluorescence
MLA	methyllycaconitine
NBQX	2,3-dihydroxy-6-nitro-7-sulfamoyl-benzo[f]quinoxaline-2,3-dione
NCX	Na^{+}-Ca^{2+} exchanger
NMDA	N-methyl D-aspartate
OGB-1	oregon green BAPTA–1
PM	plasma membrane
PPADS	pyridoxal-phosphate-6-azophenyl-2',4'-disulfonate
ROI	region of interest
RT	room temperature
RuR	ruthenium red
Rya	ryanodine
SERCA	sarcoplasmic/endoplasmic reticulum Ca^{2+} ATPase
SKF-96365	1-[β-(3-(4-Methoxyphenyl)propoxy)-4-methoxyphenethyl]-1H-imidazole hydrochloride
SOCE	store-operated Ca^{2+} entry
STIM	stromal interaction molecule

TG	thapsigargin
TIRF(M)	total internal reflection fluorescence (microscopy)
TRP	transient receptor potential
TeNT	tetanus toxin
Tx-d	Texas-Red dextran

Supplementary Experimental Procedures

Cell Culture

All experiments followed the European Union and institutional guidelines for the care and use of laboratory animals (Council directive 86/609EEC). Cortical astrocytes were prepared from P0-1 (P0 being the day of birth) NMRI mice as previously described (1). The neocortex was dissected and mechanically dissociated. Cells were plated and maintained in Petri dishes for one week to reach confluence before their transfer to cover slips (#1, BK-7, 25-mm diameter, Marienfeld Superior, Menzel-Gläser GmbH). All cultures were maintained at 37 °C in a humidified 5% CO_2 atmosphere.

Cortical neurons were isolated from embryonic mice (E16). Neurons were seeded on poly-L-lysine-treated cover slips, which were suspended above an astrocyte feeder layer and maintained in serum-free medium as described previously (2).

Culture media and recording solutions

Secondary cultures were maintained in supplemented Dulbecco's Modified Eagle Medium (DMEM, Invitrogen, ref 31885) with 5% fetal bovine serum, penicillin (5 U/ml), and streptomycin (5 µg/ml).

The standard extracellular solution contained (in mM): 140 NaCl, 5.5 KCl, 1.8 $CaCl_2$, 1 $MgCl_2$, 20 glucose, 10 HEPES (pH 7.3, adjusted with 3N NaOH). Ca^{2+}-free extracellular solutions contained nominally zero $[Ca^{2+}]_o$ and 5 mM EGTA.

Pharmacological Compounds and Fluorescent Probes

Cell media and supplements, dyes (FM1-43, FM4-64 or FM5-95, fluorescein dextran, Texas red dextran), Ca^{2+} indicator (Oregon Green BAPTA-1 AM, Xrhod-1 AM, Fluo-5N AM), and pharmacological compounds (brefeldin A and jasplakinolide) were from Invitrogen (Cergy Pontoise, France), FM3-25 from Biotium (Hayward, CA), KB-R7943 from Calbiochem (Meudon, France), GxMTx-4 from Peptides International (Louisville, KY, U.S.A.), cytochalasin D, ryanodine and thapsigargin from Tocris (Bristol, UK), BTP2, 2-APB and dynasore from Ascent Scientific (Princeton, NJ, U.S.A.), all other compounds were purchased from Sigma-Aldrich.

Dye Loading

We used several dyes with different size (3). FM5-95 (Invitrogen), a red analog of FM4-64 with the same spectral properties, has a smaller head $[(CH_3)_3N^+(CH_2)_3$ than FM4-64 $[(CH_3CH_2)_3\ N^+(CH_2)_3]$ that confers the former higher channel permeability. FM3-25, a green analog of FM1-43 with the same spectral properties, has a longer lipophilic tail (18 carbon atoms) than FM1-43 (4 carbon atoms).

We labeled astrocytes with FM1-43, FM4-64 or FM5-95 by incubating cells in a static dye-containing (6.7 μM) standard recording solution during 2-5 min, unless otherwise indicated. Staining of the external plasma membrane (PM) was washed off by thoroughly rinsing the cells for 10 min prior to imaging, unless where otherwise mentioned. When perfusing the extracellular medium at 0.5 ml/min, FM4-64 fluorescence was lost with a time constant of

25.6 ± 2.1 s (n = 8 cells). Where indicated, we quenched extracellular FM1-43 and FM3-25 fluorescence by adding 2 mM bromophenol blue (BPB).

The endocytic markers, fluorescein dextran 3,000 MW and Texas red dextran 10,000 MW , were applied in the external medium during 5 min (except Fig. S1*C* during 3 h) at 0.25 mg/ml and 0.5 mg/ml, respectively.

Recording conditions

We recorded from astrocytes in small islands of one to three cells during 2-6 days after transfer into secondary culture. During the recording session cells were constantly perfused at 0.5-1 ml/min with standard extracellular saline. During the local application of FM dyes (Fig. 5), the possible effect of the mechanical disturbance imposed by the fluid flow was controlled using a double-channel perfusion system, one channel containing the control buffer and the other the FM4-64-containing buffer (Fig. S5*A*). The different solutions were delivered through plastic tubings (0.8 mm ID, Tygon, Charny, France) to a multi-channel holder (AutoMate Scientific, Berkeley, CA) that was connected to a small (250 µm ID) silica pipette (WPI, Saratosa, Fl) positioned ~200 µm away from the cell. Switching between solutions was made in less than 5s. The effect of Gd^{3+}, GsMTx, 0 Ca^{2+}, and TG (Fig. 5*C,D*) was tested by applying the compounds both in the bath solution and in the local perfusion.

We monitored the near-membrane $[Ca^{2+}]_i$ with TIRFM using non-ratiometric Ca^{2+} indicators, Oregon Green BAPTA-1 (OGB-1, K_d ~ 170 nM) together with FM4-64/FM5-95 or Xrhod-1 (K_d ~ 700 nM) together with FM3-25. Both dyes were bulk-loaded as AM-esters (2 µM, 40 min for OGB-1; 200 nM, 15 min for Xhrod-1). Another 30 min under continuous perfusion allowed for the wash-off of membrane-bound dye and complete de-esterification. While, under these conditions, the bulk of the OGB-1 signal is derived from the cytoplasm as indicated by the complete loss of OGB-1 fluorescence in the case of PM rupture, see (1),

Xrhod-1 has a propensity to compartmentalize in mitochondria, which is also seen in our experiments by the slower and lasting Ca^{2+} signal (e.g., Fig.4*D* vs. Fig. 5*A*, and (4)).

$[Ca^{2+}]_i$ transients are plotted as dF/F_0, where F_0 is the average pre-stimulus fluorescence following subtraction of the average cellular autofluorescence measured before AM loading. Traces are corrected for photobleaching unless otherwise stated.

To directly monitor ER Ca^{2+} dynamics we used the low-affinity Ca^{2+} indicator Fluo-5N AM (5 μM, 20 min, $K_d \sim 90$ μM) that was selectively targeted to the ER lumen by over expressing a recombinant carboxylesterase with reticular targeting sequence (CES-2, the plasmid was kindly provided by Dr. Robert Blum, Ludwig-Maximilians-Universität München, Germany) (5). Transfections were done 24-36 hr prior to imaging.

In Fig.1*C*, both FM4-64 loading and dye washing was performed at 4°C in the refrigerator under local temperature control with a miniature digital thermometer (Hanna Instruments, Woonsocket, RI, U.S.A.). The cooled cell-containing chamber was transferred to the TIRF microscope and viewed at RT.

Dual-color TIRFM data (Fig. 5) were analyzed by measuring the dF/F_0 peak amplitude of the OGB-1 fluorescence and the amount of the FM4-64 retained by the cell (ΔF_{FM}).

Where indicated (Fig. 1*A*), we transiently ruptured the PM by a targeted fluid jet generated from a local perfusion pipette (~1.5 ml/min).

Imaging and Quantification

Multi-color fluorescence.

All combinations of excitation wavelengths, dichroics and filters used are listed in Table S3. We used a custom-built inverted microscope for bright-field, polychromatic epi- and through-the-objective (PlanApo TIRFM ×60, NA-1.45, Olympus, Hamburg, Germany) TIRFM (6). A Polychrome II light-source (TILL Photonics, Gräfelfing, Germany) provided monochromatic

(18-nm FWHM) epifluorescence (EPI) illumination. The 476-, 488- or 568-nm lines used for TIRFM were isolated from the beam of an Ar^+/Kr^+ multi-line laser (CVI Melles Griot, Carlsbad, CA) with an acousto-optical tunable filter (AOTF, AA.Opto, Saint. Remy-de-Chevreuse, France) and directed onto the glass/water interface at a supercritical angle. We estimated the effective penetration depth ($1/e^2$-intensity decay) of the order of 200 nm (6, 7). Fluorescence images were further magnified (×2) and projected either on an intensified camera (HighQE GenIII iPentaMax, Roper Scientific, Tucson, AZ) or an electron multiplying charge-coupled device (EMCCD, QuantEM 512, Princeton Instruments, Trenton, NJ) camera, both controlled by Metamorph (Molecular Devices, Downingtown, PA). Effective pixel sizes in the sample plane were 187 nm and 133 nm, for the two cameras, respectively. Time-lapse image stacks were taken at 1 Hz with 50-300 ms exposure times.

We systematically calculated the amount of cross-talk in multi-color imaging experiments using measured *in vitro* spectra (8). Additionally, we always imaged control astrocytes containing only one of the fluorophores in all imaging channels to experimentally exclude cross-talk (e.g., Fig. S5). Co-localization was assessed similar to (1), by calculating Pearson's correlation coefficient, r_{12}, which evaluates the spatial correlation of dual-color images by using the information of all pixels. The upper meaningful limit (+CTR) of our correlation analysis was determined by the virtually complete overlap between FM1-43 and FM4-64 in double-labeled astrocytes ($r_{12} = 0.90 \pm 0.03$, $n = 7$; Fig. S1*A*). The lower limit (-CTR) was calculated from scrambled red/green-channel image regions of interest (ROIs) taken from different double-labeled cells ($r_{12} = 0.06 \pm 0.02$, $n = 8$). Co-localization quantification were performed with images of comparable signal-to-noise ratio (SNR, between 12 and 15 (1)).

Image filtering, segmentation, particle density and single-spot measurements

We measured the density of fluorescent organelles after high-pass filtering (1 μm^{-1} cut-off), thresholding the image with a systematic 10%-of-peak-intensity criterion, and watershed segmentation (with ImageJ, NIH and Metamorph 7.0, Molecular Devices). Particle number was normalized with total area, estimated for epifluorescence images from the thresholded contour of the cell and for TIRF images from the size of the region of interest (ROI) analyzed.

Finally, to be counted as an object, a FM dye-labeled punctum had to be detected in the ROI under study (using single-spot spectral emission imaging (6)) and it had to comprise at least 2×2 pixels. Mean fluorescence (MF) of single cells was measured within the contour, after subtraction of the average mean autofluorescence measured in the corresponding color channel from non-labeled cells of the same preparation. For each pharmacological condition, control and treated measurements of MF and particle density were performed on paired cells from the same preparation.

Evolution with time of fluorescence in small ROIs (e.g., Fig. 1*A*) was measured as the mean value in a 1 μm-diameter region, centered either on a spot, localized in a spot-free cytoplasmic region or in the extracellular space. Cytoplasmic fluorescence traces are shown after the subtraction of extracellular background, whereas the ROIs containing a labeled organelle are subtracted with the local background measured in a concentric annulus with a 1.4 μm outer diameter (1).

Statistics

All data are expressed as mean ± standard deviation (SD), and the *t*-test was used for testing the significance of *P* values. Non-normally distributed data were compared using their median ± absolute deviation and non-parametric tests (Kolmogorov-Smirnov, KS). All statistical operations used Matlab (The MathWorks). $*p < 0.05$, $**p < 0.01$, $***p < 0.001$.

Table S1. Involvement of Ca^{2+} permeable channels and exchangers in FM4-64 uptake

	Conc (μM)	MF (a.u.)*	p^{+}	Puncta/μm²	$p^{\S}$	$n^{£}$	*Channel/exchanger targeted*
CTR	-	1	.	1	.	24	
NBQX	5	94.6 ± 49.6%	0.48	106.9 ± 41.7%	0.42	14	AMPAR (antagonist) (9)
d-AP5	10	84.9 ± 35.2%	0.28	94.4 ± 38.9%	0.45	11	NMDAR (antagonist) (10)
ATP	50	108.9 ± 31.9%	0.58	97.2 ± 41.7%	0.65	9	P2X (agonist) (11)
PPADS	100	106.9 ± 44.6%	0.58	93.1 ± 40.7%	0.28	16	P2X (antagonist) (11)
MLA	0.01	120.3 ± 61.1%	0.22	95.8 ± 55.6%	0.7	14	α7-containing acetylcholine receptor (AchR) (antagonist) (12)
Co^{2+}	100	91.9 ± 30.5%	0.44	94.4 ± 41.7%	0.48	12	Voltage-gated Ca^{2+} channel (antagonist) (13)
nifedipine	5	106.7 ±30.3%	0.67	90.3 ± 27.8%	0.2	11	Voltage-gated Ca^{2+} channel (blocker) (13)
Ba^{2+}	100	94.2 ± 39.0%	0.63	101.4 ± 41.7%	0.98	11	Kir4.1(antagonist) (14)
DHS	100	104.2 ± 34.2%	0.93	95.8 ± 27.8%	0.45	10	Mechanotransducer channel (blocker) (15)
RuR	10	99.1 ± 15.5%	0.97	102.8 ± 35.5%	0.97	18	TRPV (antagonist) (16)
CBX	100	86.8 ± 33.4%	0.29	104.2 ± 41.7%	0.8	17	Hemichannel (blocker) (17)
FFA	100	110.9 ± 36.0%	0.43	102.8 ± 55.6%	0.89	12	Volume-sensitive anion channel (blocker) (18)
KB-R7943	5	91.9 ± 32.2%	0.55	95.8 ± 34.7%	0.77	10	Na^{+}-Ca^{2+} exchanger (inhibitor) (19)
2-APB	100	235.1 ± 81.9%	0.0006	157.1 ± 57.1%	0.0062	16	Orai1 blocker (20, 21)

* MF and particle density are reported as percentage of their respective paired controls

$^{+}$ MF is expressed as median ± SD and significance of difference evaluated by Kolmogorov-Smirnov test

§ Puncta/μm² is expressed as mean ± SD and significance of difference evaluated by *t* test

$^{£}$ *n*, number of cells

Table S2. Involvement of store-operated Ca^{2+} entry pathway in FM4-64 uptake

	Conc	MF (a.u.)[+]	p[+]	N[+]	Puncta/µm²[§]	p[§]	n[§]
CTR*	-	98.0 ± 62.5	.	20	0.07 ± 0.02	.	11
TG*	2 µM	279.7 ± 223.8	< 0.01	21	0.11 ± 0.04	< 0.01	12
CTR	-	130.6 ± 61.6	.	16	0.06 ± 0.02	.	16
Calyculin A	200 nM	651.5 ± 335.7	< 0.01	8	0.03 ± 0.03	< 0.05	8
CTR	-	68.6 ± 27.7	.	24	0.08 ± 0.03	.	9
Anisomycin	30 µM	36.1 ± 32.2	< 0.05	22	0.03 ± 0.02	< 0.01	9
CTR	-	198 ± 69.9	.	18	0.07 ± 0.02	.	18
Gd^{3+}	100 µM	9.97 ± 8.1	< 0.01	18	0.01 ± 0.01	< 0.01	18
CTR	-	198.0 ± 69.8	.	15	0.07 ± 0.02	.	9
BTP2	40 µM	55.7 ± 38.8	< 0.01	20	0.02 ± 0.01	< 0.01	9
CTR	-	635.3 ± 172	.	22	0.08 ± 0.03	.	22
SKF96365	20 µM	390.8 ± 141.8	< 0.01	27	0.06 ± 0.03	< 0.05	27
CTR	-	443.4 ± 190.2	.	16	0.08 ± 0.03	.	16
GsMTx-4	5 µM	190.2 ± 71.4	< 0.01	15	0.05 ± 0.02	< 0.05	15
CTR	-	391.3 ± 118.1	.	15	0.07 ± 0.03	.	15
LPC	5 µM	3530.7 ± 1310.4	< 0.001	16	0.11 ± 0.05	< 0.05	16
CTR	-	1035.2 ± 375.2	.	13	0.07 ± 0.03	.	13
MβCD	10 mM	265.8 ± 253.7	< 0.01	15	0.04 ± 0.02	< 0.05	15

* The effect of a pharmacological compound was estimated by comparing experimental (TG, Calyculin A, etc.) with control (CTR) coverslips from same culture batch.

[+] MF is expressed as median ± SD; *p*, significance of difference evaluated by Kolmogorov-Smirnov test; *n*, number of cells.

[§] Puncta/µm² is expressed as mean ± SD; *p*, significance of difference evaluated by *t* test; *n*, number of cells.

Table S3. Combinations of filters, fluorescent probes and settings used for multi-color imaging

Dye(s)	Epifluorescence (EPI)			TIRFM		
	ex* (nm)	DC (nm)	em (nm)	ex+ (nm)	DC (nm)	em (nm)
FM1-43	488	500	560(40)BP or 615(45)BP	488	500	560(40)BP or 615(45)BP
FM3-25	488	500	560(40)BP or 615(45)BP	488	500	560(40)BP or 615(45)BP
FM4-64	488	500	675(50)BP	488	500	675(50)BP
FM5-95	488	500	675(50)BP	488	500	675(50)BP
OGB-1	488	500	535(50)BP	488	500	535(50)BP
Xrhod-1				568	PolyX§	675(50)BP
FM1-43 & FM4-64				476	500	560(40)BP & 675(50)BP$
FM4-64 & OGB-1				488	500	535(50)BP & 675(50)BP$
FM4-64 & Fluo5N				488	500	535(50)BP & 675(50)BP$
FM4-64 & FL-d				488	500	535(50)BP & 675(50)BP$
FM1-43 & TX-d				488 & 568	PolyX	615(45)BP

*center wavelength of the 18-nm (FWHM) excitation band of a TILL polychrome II tunable light-source.

+wavelengths designate the lines of an Ar^+/Kr^+ mixed-gas laser, selected by an acousto-optical tunable filter.

§PolyX – a custom dual dichroic mirror with 488/568/NIR reflection bands and low ripple high-transmission elsewhere (AHF Analysentechnik).

$ denotes filters for simultaneous view with a custom dual-view device.

Supplementary Figures

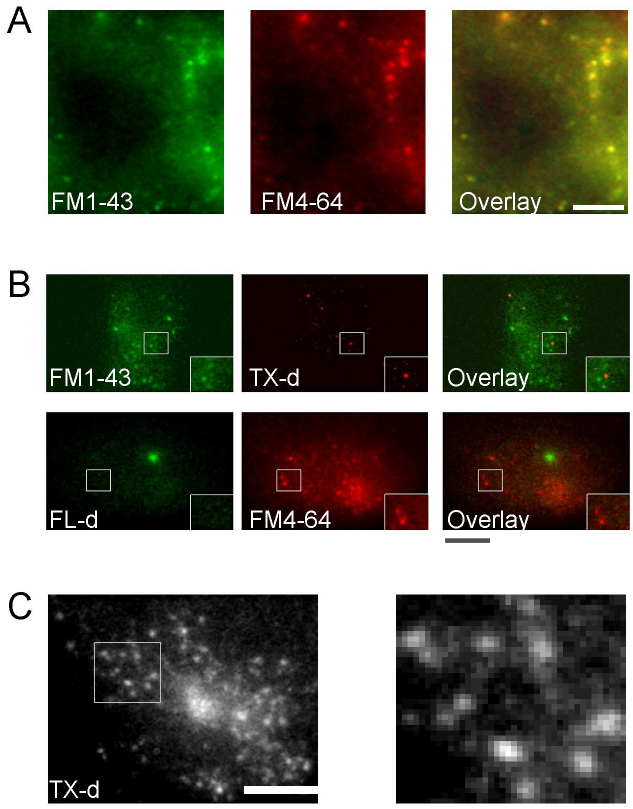

Fig. S1. Astrocytic FM1-43 or FM4-64 labeling does not overlap with endocytic markers

(*A*) TIRF images of an astrocyte co-labeled with FM1-43 and FM4-64 (6.7 μM for each, 10 min). Scale bar, 5 μm. (*B*) Dual-color TIRF images of astrocytes co-labeled with either FM1-43 or FM4-64 and a spectrally matched endocytic marker. The green-emitting FM1-43 (6.7 μM) and the red endocytic marker Texas red dextran 10,000 MW (TX-d, 0.5 mg/ml) were excited alternately at 488- and 568-nm, and the red-emitting FM4-64 and the green endocytic marker fluorescein dextran 3,000 MW (FL-d, 0.25 mg/ml) at 488-nm. Bars, 10 μm. (*C*) The long-term loading with the endocytic marker TX-d (0.5 mg/ml, 3 hr) resulted in punctuate fluorescence. The boxed area is shown at higher magnification (*right*). Similar result was obtained with FL-d (0.25 mg/ml, 3 hr, not shown). Bar, 10 μm.

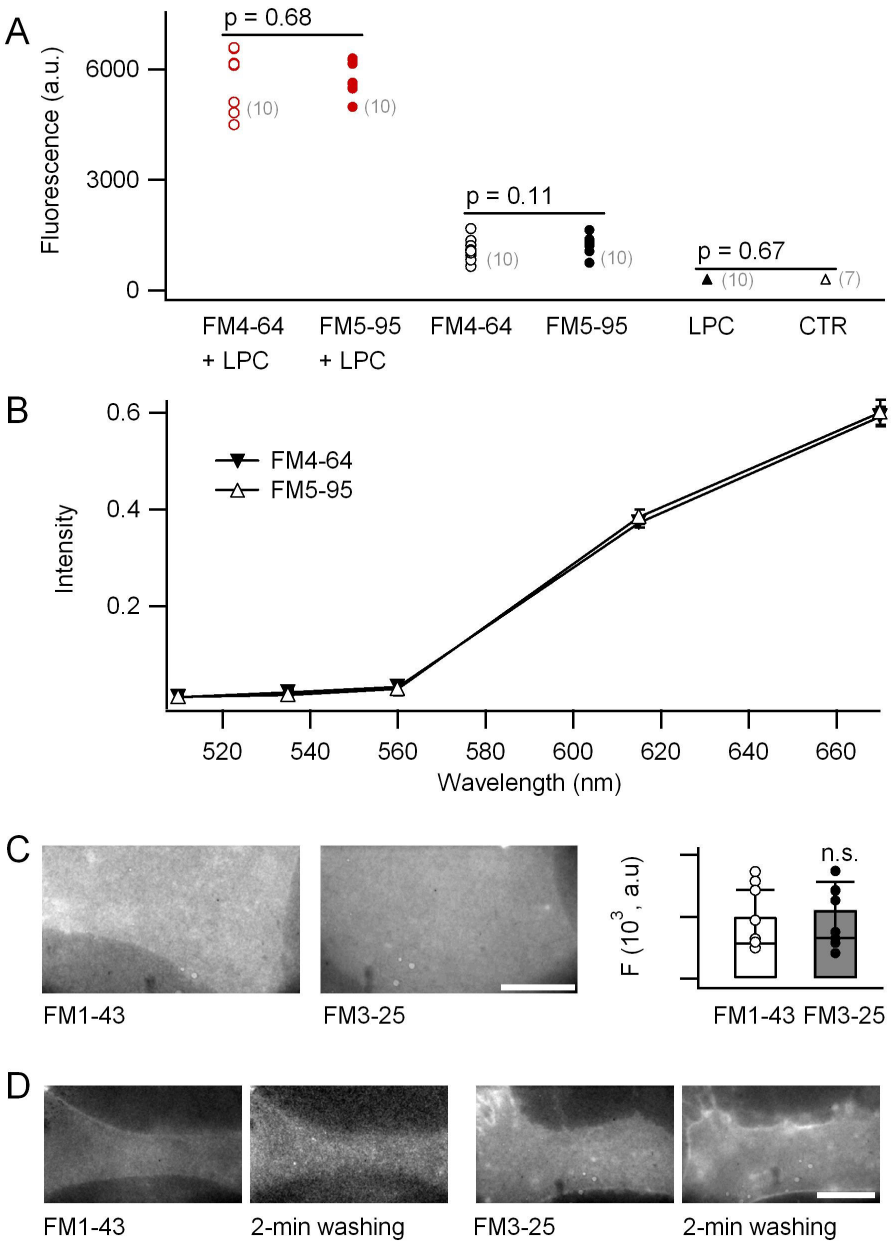

Fig. S2. Quantitative comparison of FM4-64/FM5-95 and FM1-43/FM3-25 fluorescence

(*A*) FM4-64 and FM5-95 display similar fluorescence under different conditions. The addition of 50 μM lysophosphatidylcholine (+LPC) to form lipid micelles provides a hydrophobic environment for FM4-64 and FM5-95. Numbers in parentheses indicate the number of trials. (*B*) Experimentally determined 5-point emission spectra of LPC-bound FM4-64 and FM5-95, respectively (n = 7 measurements for each, error bars represent standard deviation, $P > 0.7$ for each data point). During spectral imaging, FM4-64 and FM5-95 were excited by 458-nm light

and the emitted fluorescence collected consecutively by five narrow-band emission filters (510-nm, 535-nm, 560-nm, 615-nm and 670-nm). Spectra were corrected for extracellular background, B_{ex}, taken with the same imaging parameters in a cell-free region, normalized to equal energy, $\sum_{i=1}^{5} S_i = 1$, and averaged (see details in ref 5). (*C*) *Left*, example EPI images of the plasma membrane labeling of astrocytes incubated in 12 μM FM1-43 and 20 μM FM3-25, respectively. Bar, 10 μm. *Right*, similar cell surface labeling for both conditions (n = 8 – 9, p = 0.84). (*D*) Representative epifluorescence images showing that FM1-43 dye departitions from the outer leaflet of the plasma membrane during a 2-min wash (global perfusion, ~0.5 ml/min), while no obvious decrease was observed for the more sticky FM3-25, even after 20 min of wash. Bar, 10 μm.

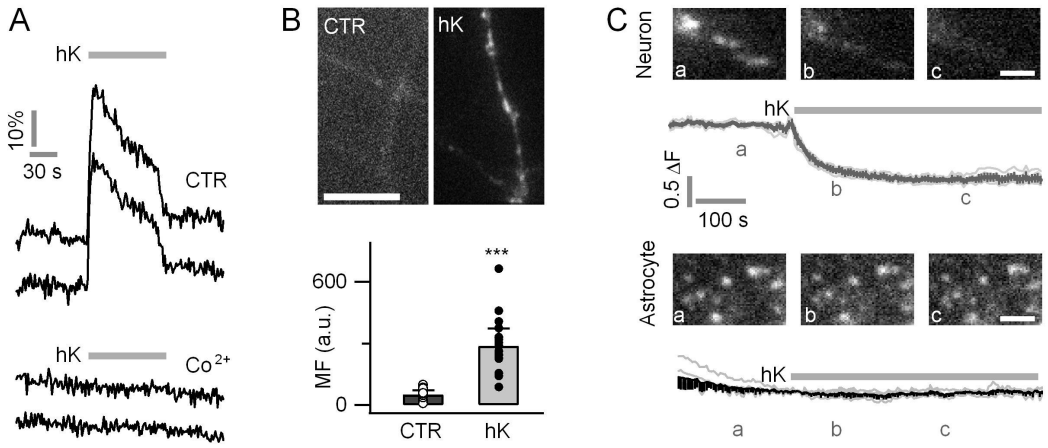

Fig. S3. High K^+ enhances FM4-64 uptake and triggers exocytosis in neurons, but not astrocytes.

(*A*) Astrocyte $[Ca^{2+}]_i$ elevation evoked by high $[K^+]_o$ (hK, 60 mM). Calcium transients were imaged by TIRFM using the Ca^{2+} fluorescent dye OGB-1, AM. 2 mM Cobalt (Ca^{2+}) totally inhibited the response. Same results were obtained for $[K^+]_o$ ranging from 20 mM – 120 mM. (*B*) Cortical neuronal cultures labeled by FM4-64 (6.7 μM, 2 min) in control and high-potassium (hK, 120 mM) conditions, confirm the well-documented activity-dependent FM4-64 internalization. n = 18–26 cells per condition. Scale bar, 10 μm. ***p<0.001. (*C*) Neuronal FM4-64 labeling was removed by high potassium solution (hK, 60 mM, n = 9 labeled sub-regions), to which astrocytic FM4-64 staining was resistant (n = 6 labeled sub-regions). Scale bar, 5 μm.

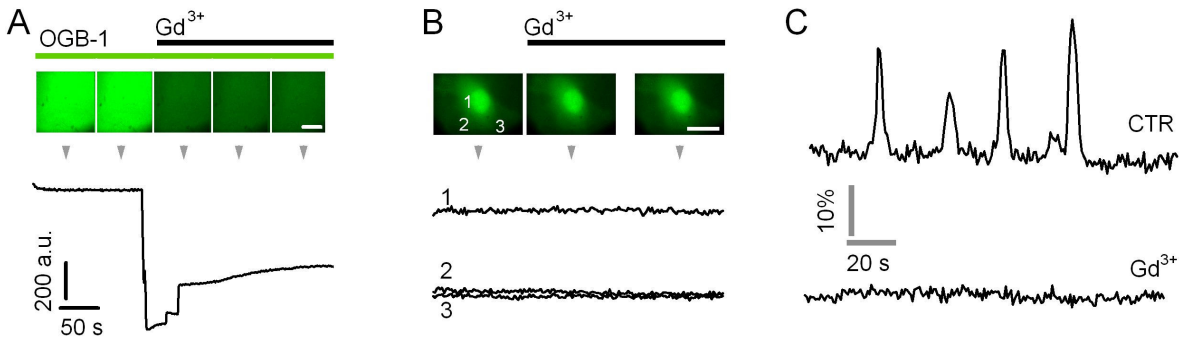

Fig. S4. Gd^{3+} inhibits spontaneous astrocyte Ca^{2+} oscillations

Gd^{3+} is a blocker of SOCE (22). We examined its effect on spontaneous astrocyte Ca^{2+} oscillations which are sustained by the basal activity of the channels implicated in SOCE (23). (*A*) As we observed that Gd^{3+} quenches OGB-1 fluorescence *in vitro*, we first probed the effect of adding of 100 µM Gd^{3+} to a solution containing 10 µM OGB-1 and 50 µM Ca^{2+}. Indeed, the addition of Gd^{3+} resulted in an instantaneous decrease in OGB-1 fluorescence (dF/F_0 = 83.7 ± 6.7 %, *n* = 3 trials). *Top*, Images acquired at times indicated by grey arrows. *Bottom*, time course of OGB-1 fluorescence. Scale bar, 10 µm. (B) In contrast, astrocyte-loaded OGB-1 is protected from Gd^{3+} quenching, indicating that Gd^{3+} does not enter the cytoplasm. *Top*, Images of an OGB-1 loaded astrocyte (2 µM, 40 min) before and after the addition of 100 µM Gd^{3+}. Traces (1)-(3) plot different subcellular ROIs. Bar, 20 µm. (C) Spontaneous $[Ca^{2+}]_i$ oscillations recorded from OGB-1-loaded astrocytes were completely abolished upon addition of extracellular Gd^{3+} (100 µM). In 12 out of 19 cells displaying spontaneous Ca^{2+} oscillations at a rate of 1.1 ± 0.4 transients/min, activity was inhibited by 100 µM Gd^{3+} confirming the role of SOCE in these spontaneous signals. As expected from a SOCE-dependent dye entry, Gd^{3+} also abolished FM4-64 uptake (Fig. 3).

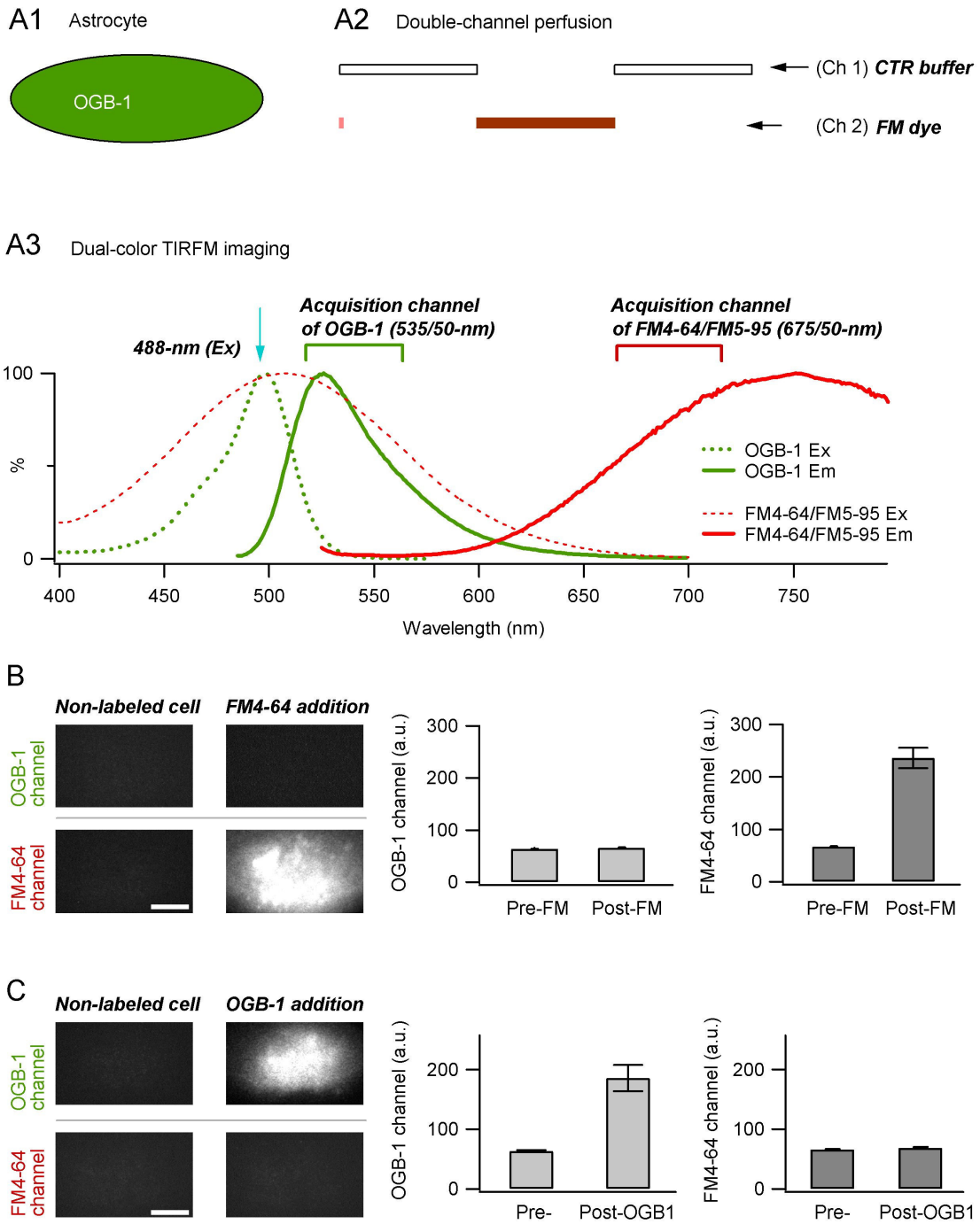

Fig. S5. Single-color excitation dual-color emission detection of FM4-64 and OGB-1 allow the detection of FM4-64-triggered astrocytic Ca^{2+} signals

(*A*) Astrocytes were preloaded with the green fluorescent Ca^{2+} indicator OGB-1 (2 µM, 40 min, *A*1). The CTR buffer and the buffer containing the red-emitting FM4-64 was separately and locally applied to the target cell through a small diameter (100 µm ID) silica pipette

connected to a small diameter (250 μm ID) silica needle (MicroFil 28GAWG, World Precision, Sarasota, FL, USA), cut at 4 cm and attached to a Perfusion Pencil® Multi-Barrel Manifold Tip (Automate Scientific, Berkeley, CA, USA). The perfusion at 0.4 ml/min was maintained with a peristaltic pump (Ismatec). *In vitro* spectra of OGB-1 and FM4-64 predict little crosstalk (*A*3), as confirmed on live-cell images (*B*-*C*). Application of FM4-64 resulted in pronounced fluorescence increase in the red channel but little, if any, change in the green channel (n = 8 cells per condition; B). The opposite effect was observed when loading OGB-1 only (C). n = 6 cells per condition. Scale bars, 10 μm.

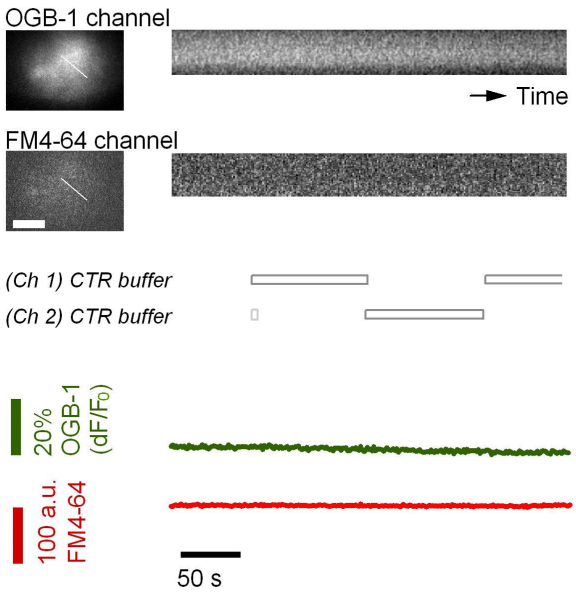

Fig. S6. Only applying control buffer does not induce $[Ca^{2+}]_i$ changes in astrocytes.

Little, if any, $[Ca^{2+}]_i$ change ($dF/F_0 = 0.01 \pm 0.02$, $n = 11$ cells), was observed when applying through the perfusion channel 2 (*Ch 2*) the control buffer (i.e., without FM4-64). *Top left*, an example dual-color image of astrocytes pre-loaded with the green calcium dye OGB-1 AM. *Top right*, kymographs displaying the evolution with time of the fluorescence profile measured along the white lines placed on OGB-1 and FM4-64 image, respectively. *Middle*, only control buffer was applied through *Ch2* following the perfusion protocol described in Fig. S5. *Bottom*, no appreciable calcium response was observed in astrocytes, thus excluding an influence of the perfusion system itself on the measured $[Ca^{2+}]_i$.

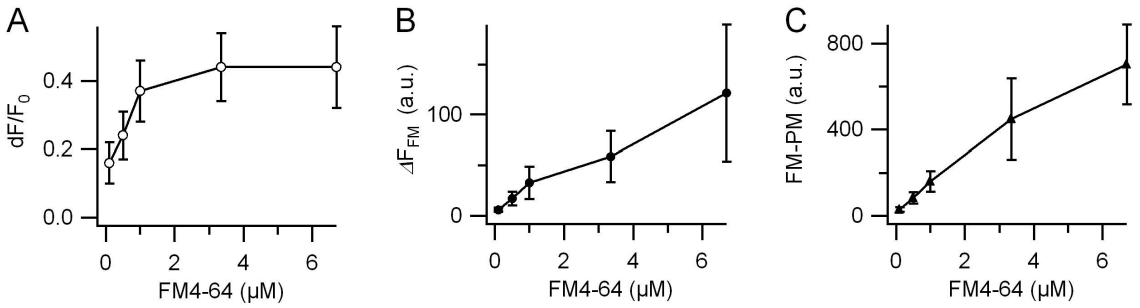

Fig. S7. Concentration dependence of the effect of FM4-64.

Several concentrations of FM4-64 (0.1, 0.5, 1, 3.35, 6.7 μM, n = 8, 9, 9, 8, 9 cells, respectively) were applied to OGB-1-loaded astrocytes following the same protocol as in Fig. 5. The peak $[Ca^{2+}]_i$ increase (dF/F_0, *A*), the residual fluorescence measured at the end of the 2 min FM4-64 wash (ΔF_{FM}, ***C***, see details in the main text), and the PM fluorescence measured at the end of the 90-s FM4-64 application (FM-PM, *C*) are shown as a function of FM4-64 concentration. The concentration of FM4-64 (6.7 μM) used in our study that induces a submaximal dye insertion in the PM (FM-PM) and FM uptake (ΔF_{FM}) triggered a maximal $[Ca^{2+}]_i$ increase.

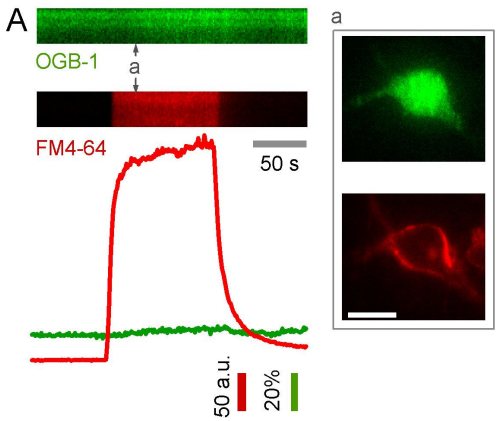

Fig. S8. Unlike astrocytes, neurons show little FM4-64-triggered Ca^{2+} increases

A weak $[Ca^{2+}]_i$ change (dF/F_0 = 0.03 ± 0.1, n = 7 cells, p<0.01) was observed upon the application of FM4-64 (6.7 µM) to a OGB-1-loaded cortical neuron. *Inset a*, representative dual-color TIRF images acquired 18 s after FM4-64 application. Scale bar, 10 µm.

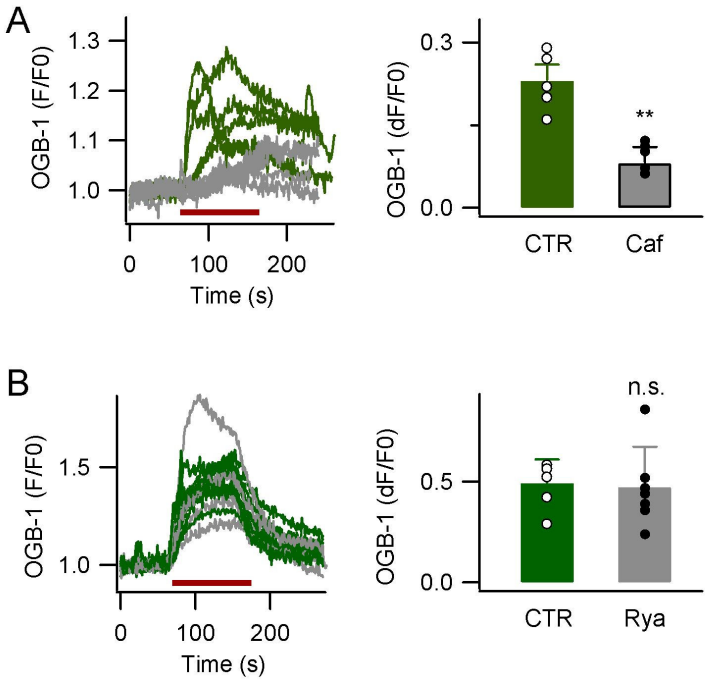

Fig. S9. Inhibiting by caffeine (Caf, 10 mM) the rate of opening of IP_3R Ca^{2+} channels down-regulates FM4-64-elicited $[Ca^{2+}]_i$ response.

(*A*) *Left*, Superimposed FM4-64-triggered responses from control (*green*) and caffeine-treated cells (*grey*), respectively. Red bar indicates the FM4-64 application. (*B*) Pre-discharging the ryanodine (Rya)-sensitive internal store (1 μM ryanodine, 60 min, (24)) did not affect Ca^{2+} response to FM4-64 application (6.4 μM, 90 s). *Left*, FM4-64-evoked Ca^{2+} responses pooled from control (*green*) and Rya-treated cells (*grey*), respectively. Red bar times FM4-64 application.

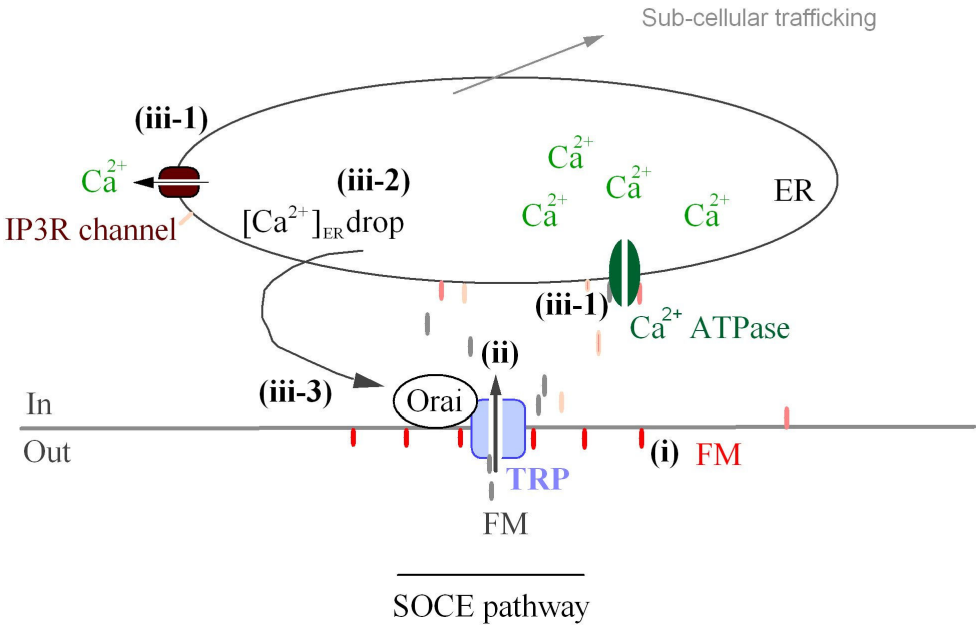

Fig. S10. Scheme illustrating the triple action exerted by permeant FM dyes on astrocytes.

(*i*) The FM dye partitions into the outer leaflet of the PM where it facilitates the activation of the SOCE pathway in a lipid bilayer-dependent manner; (*ii*) by competing with Ca^{2+} for permeating across SOCs, the permeant blocker FM dyes interfere with SOCE and reduces Ca^{2+} influx across the PM; (*iii*) the permeant FM dyes, once in the cytosol, alter the gating of IP_3R channels and change the ER Ca^{2+} ATPase activity (*iii-1*), mobilizes Ca^{2+} from ER store (*iii-2*), conveying a positive feed-back signal to activate SOCE (*iii-3*), and sustain the FM dye uptake into astrocytes.

Supplementary references

1. Li D, Ropert N, Koulakoff A, Giaume C, Oheim M (2008) Lysosomes are the major vesicular compartment undergoing Ca^{2+}-regulated exocytosis from cortical astrocytes. *J Neurosci* 28:7648-7658.
2. Kaech S, Banker G (2006) Culturing hippocampal neurons. *Nat Protoc* 1:2406-2415.
3. Betz WJ, Mao F, Smith CB (1996) Imaging exocytosis and endocytosis. *Curr Opin Neurobiol* 6:365-371.
4. Gerencsér ÁA, Adam-Vizi V (2001) Selective, high-resolution fluorescence imaging of mitochondrial Ca^{2+} concentration. *Cell Cal* 30:311-321.
5. Rehberg M, Lepier A, Solchenberger B, Osten P, Blum R (2008) A new non-disruptive strategy to target calcium indicator dyes to the endoplasmic reticulum. *Cell Cal* 44:386-399.
6. Nadrigny F, et al. (2006) Detecting fluorescent protein expression and co-localisation on single secretory vesicles with linear spectral unmixing. *Eur Biophys J* 35:533-547.
7. Nadrigny F, et al. (2007) Systematic colocalization errors between acridine orange and EGFP in astrocyte vesicular organelles. *Biophys J* 93:969-980.
8. Oheim M, Li D (2007) in Imaging Cellular and Molecular Biological Functions, eds. Shorte SL, Frischknecht F (Springer, Heidelberg), pp 117-156.
9. Seifert G, Weber M, Schramm J, Steinhäuser C (2003) Changes in splice variant expression and subunit assembly of AMPA receptors during maturation of hippocampal astrocytes. *Mol Cell Neurosci* 22:248-258.
10. Lalo U, Pankratov Y, Kirchhoff F, North RA, Verkhratsky A (2006) NMDA receptors mediate neuron-to-glia signaling in mouse cortical astrocytes. *J Neurosci* 26:2673-2683.
11. Lalo U, et al. (2008) P2X1 and P2X5 subunits form the functional P2X receptor in mouse cortical astrocytes. *J Neurosci* 28:5473-5480.
12. Sharma G, Vijayaraghavan S (2001) Nicotinic cholinergic signaling in hippocampal astrocytes involves calcium-induced calcium release from intracellular stores. *Proc Natl Acad Sci US A* 98:4148-4153.
13. Latour I, Hamid J, Beedle A, Zamponi G, Macvicar B (2003) Expression of voltage-gated Ca^{2+} channel subtypes in cultured astrocytes. *Glia* 41:347-353.
14. Härtel K, et al. (2007) Calcium influx mediated by the inwardly rectifying K^+ channel Kir4.1 (KCNJ10) at low external K^+ concentration. *Cell Cal* 42:271-280.
15. Marcotti W, van Netten SM, Kros CJ (2005) The aminoglycoside antibiotic dihydrostreptomycin rapidly enters mouse outer hair cells through the mechano-electrical transducer channels. *J Physiol* 567:505-521.
16. Ramsey I, Delling M, Clapham D (2006) An introduction to TRP channels. *Annu Rev Physiol* 68:619-647.
17. Thompson RJ, Zhou N, MacVicar BA (2006) Ischemia opens neuronal gap junction hemichannels. *Science* 312:924-927.
18. Takano T, et al. (2005) Receptor-mediated glutamate release from volume sensitive channels in astrocytes. *Proc Natl Acad Sci US A* 102:16466-16471.

19. Hirota S, Pertens E, Janssen LJ (2007) The reverse mode of the Na^+/Ca^{2+} exchanger provides a source of Ca^{2+} for store refilling following agonist-induced Ca^{2+} mobilization . *Am J Physiol Lung Cell Mol Physiol* 292:L438-447.

20. Feske S, et al. (2006) A mutation in Orai1 causes immune deficiency by abrogating CRAC channel function. *Nature* 441:179-185.

21. Zhang SL, et al. (2008) Store-dependent and -independent modes regulating Ca^{2+} release-activated Ca^{2+} channel activity of human orai1 and orai3. *J Biol Chem* 283:17662-17671.

22. Ju Y-K, et al. (2007) Store-operated Ca^{2+} influx and expression of TRPC genes in mouse sinoatrial node. *Circ Res* 100:1605-1614.

23. Singaravelu K, Lohr C, Deitmer JW (2006) Regulation of store-operated calcium entry by calcium-independent phospholipase A_2 in rat cerebellar astrocytes. *J Neurosci* 26:9579-9592.

24. Golovina V, Blaustein M (2000) Unloading and refilling of two classes of spatially resolved endoplasmic reticulum Ca^{2+} stores in astrocytes. *Glia* 31:15-28.